Relation between cathodoluminescence and trace element distribution of magmatic topaz from the Ary-Bulak massif, Russia

Andrea Agangi[a,b,*], Arnold Gucsik[a], Hirotsugu Nishido[c], Kiyotaka Ninagawa[d], Vadim S. Kamenetsky[e]

[a] Department of Geology, University of Johannesburg, Auckland Park 2006, South Africa

[b] Department of Applied Geology, Curtin University, Bentley 6102 WA, Australia

[c] Department of Applied Physics, Okayama University of Science, Okayama, Japan

[d] Research Institute for Natural Sciences, Okayama University of Science, Okayama, Japan

[e] School of Physical Sciences, University of Tasmania, Hobart TAS 7001, Australia

* Corresponding author andrea.agangi@curtin.edu.au (A. Agangi)

agucsik@uj.ac.za (A. Gucsik), kninagawa@dap.ous.ac.jp (K. Ninagawa), nishido@big.ous.ac.jp (H. Nishido), dima.kamenetsky@utas.edu.au (V. Kamenetsky)

Abstract

In order to define the cathodoluminescence properties of magmatic topaz and its relations with trace element composition, we studied topaz phenocrysts from the Ary-Bulak ongonite massif, Russia using a wide array of analytical techniques. SEM-CL panchromatic images reveal strong variations, which define micrometer-scale euhedral growth textures. Several truncations of these growth textures occur in single grains implying multiple growth and resorption events. CL spectra of both CL-bright and -dark domains have a major peak in the near-ultraviolet centered at 393 nm. CL images taken after several minutes of electron bombardment show decreasing emission intensity. Electron microprobe analyses indicate high F concentrations (average OH/(OH + F) = 0.04 calculated by difference, 100 wt% – EPMA tot), consistent with what has been previously found in topaz-bearing granites, and the OH stretching vibration (~3653 cm^{-1}) was detected in Raman spectra. Laser ablation ICP-MS traverses performed across the CL textures detected trace elements at ppm to thousands of ppm levels, including Fe, Mn, Li, Be, B, P, Nb, Ta, W, Ti, Ga, light rare earth elements, Th, U. Lithium, W, Nb and Ta appear to be correlated with CL intensity, suggesting a role for some of these elements in the activation of CL in topaz. In contrast, no clear correlation was found between CL intensity and F contents, despite the fact that the replacement of OH for F is known to affect the cell parameters of topaz.

Key words

40 Topaz; fluorine; lithium; ongonite; cathodoluminescence; Raman; rare
41 metals

42

Introduction

Topaz [$Al_2SiO_4(F,OH)_2$] is a typical mineral in F-rich, strongly fractionated magmas, which are emplaced at shallow depth forming pegmatites and microgranites, or erupted as volcanic rocks (e.g. Payette and Martin, 1990; Thomas et al., 2009; London and Kontak, 2012; Thomas and Davidson, 2013;). Topaz typically crystallizes in the orthorhombic system (space group Pbnm), and its structure consists of SiO_4 groups linking octahedral zig-zag chains of $Al[O_4(F, OH)_2]$ parallel to the c-axis. Four of the anions forming Al octahedra are oxygens, and other two are F or OH groups. In magmatic systems, topaz is stabilized in peraluminous, low-Ca compositions, and at F contents of more than 2 – 3 wt% (Congdon and Nash, 1988), or more than 1 wt% (Burt et al., 1982). This type of magmas is commonly associated with ore deposits including rare-metals (e.g. Ta, Nb, W), Li, F, Sn and Mo (Burt et al., 1982; Manning and Hill, 1990; Taylor, 1992; Raimbault et al., 1995; Charoy and Noronha, 1996; Williams-Jones et al., 2000; Bradley and McCauley, 2013; Bastos Neto et al., 2014), some of which are crucial in modern high-technology applications (USGS, 2011; London and Kontak, 2012; RMSG, 2014).

Cathodoluminescence (CL) microscopy and spectroscopy have been applied as powerful methodologies to the earth and planetary sciences for several decades (e.g., Williams and Yoffe, 1969; Hayward, 1988; Pagel et al., 2000; Gucsik, 2009; Götze, 2012; and references therein). CL can reveal crystallization textures that cannot be observed with other techniques such as

optical microscopy and secondary electron or backscattered electron imaging. In magmatic systems, CL can be used to identify zoning patterns, primary and secondary crystallization stages and resorption features in different minerals (Müller et al., 2000; Song and Yuan, 2009; Agangi et al., 2011; Vasyukova et al., 2013). Despite recent studies (MacRae and Wilson, 2008; Song and Yuan, 2009; Correcher et al., 2011), the luminescence characteristics of natural topaz are still poorly understood. In a pioneering study, Gaft et al., (2005) investigated Mn, V, Cr, and Ti as activator elements in laser-induced luminescence of topaz samples by time-resolved spectroscopy. They found that Cr^{3+} plays a key role as a CL color center not only in yellow but also red luminescing topaz. Neutron and gamma-ray irradiation are known to modify color centers of topaz enhancing the blue color (da Silva et al., 2005; Krambrock et al., 2007; Zhang et al., 2011). Luminescent centers in topaz and their assignment are summarized in Table 1.

A better knowledge of the geochemical and luminescence properties of topaz may lead to its application to the study of magma evolution, similarly to what has been done for quartz (e.g. Götze et al., 2001; Müller et al., 2002; Breiter, 2009). For example, it has been recently shown that trace element zoning and related CL variations can be potentially used as a proxy for trace element fluctuations in the parent melt during topaz crystallization (Agangi et al., 2014).

In order to better define the CL properties of magmatic topaz and their relation to the trace element composition, we studied a sample of F-rich, topaz-

phyric rhyolite (known as ongonite) from the central part of the Ary-Bulak massif (sample AB1). The CL, microchemical and microtextural characteristics of the sample have been studied with a multiple approach, which includes optical microscopy, back-scattered electron (BSE) and cathodoluminescence (CL) modes of scanning electron microscopy (SEM), laser ablation ICP-MS (LA-ICP-MS), micro-Raman spectroscopy and FTIR.

Geological setting and sample description

The 142 ±0.7 Ma old (Kostitsyn et al., 1996) Ary-Bulak massif forms a laccolith, 700 x 1500 m in size, intruding Late Jurassic-Early Cretaceous shales and limestones of the Ust'-Boryza Formation and basalt (Kovalenko and Kovalenko, 1976; Antipin et al., 2009; Peretyazhko and Savina, 2010a). The massif is concentric with a center consisting of porphyritic ongonite with up to 20 vol.% phenocrysts of sanidine, albite, quartz, Li-mica (zinnwaldite) and occasional topaz. To the southwest, the porphyritic rocks grade into an aphanitic variety of ongonite, which forms a quenched contact zone up to 100 m wide (Peretyazhko et al., 2011). Whole-rock analyses indicate strong enrichment in Nb, Ta, W, Sn, Li and Rb in comparison with continental crust (e.g. up to 73 ppm Nb, 48 ppm Ta, 30 ppm W, respectively), and typically flat or concave upwards primitive-mantle normalized rare earth element (REE) patterns with pronounced negative Eu anomalies (e.g. Syritso et al., 2012). The massif was emplaced at the same time as other shallow intrusions of similar composition in Eastern Transbaikalia (Khrangilay complex, Badanina et al., 2006). Complex

assemblages of quartz- and topaz-hosted silicate melt inclusions and immiscible saline fluids, brines and fluoride melts have been described and analyzed in several studies (Peretyazhko et al., 2007; Peretyazhko and Savina, 2010a, 2010b; Agangi et al., 2014).

Sample AB1 is a porphyritic rock with phenocrysts of smoky quartz, K-feldspar, Na-plagioclase, topaz and mica (Fig 1A) embedded in quartz-feldspar-topaz groundmass. All minerals are very fresh, feldspar and topaz are water-clear and lack any sericite alteration. Topaz forms euhedral, colorless, prismatic and locally splinter-shaped, phenocrysts up to 1-2 mm long. Topaz phenocrysts contain abundant inclusions of feldspar, aggregates of Nb-Ta-W oxide (W-ixiolite to tantalite-columbite), mica, round grains of quartz, and elongate to irregular grains of cryolithionite [$Na_3Li_3Al_2F_{12}$]. A detailed sample description is given in Agangi et al. (2014).

Analytical techniques

Cathodoluminescence (CL)

Panchromatic scanning electron microscope cathodoluminescence (SEM-CL) images were obtained using a Tescan Vega 3 electron microscope equipped with a CL detector at the Spectrum Centre of the University of Johannesburg. The accelerating voltage was 20 kV.

CL color imaging was carried out using a Luminoscope (ELM-3R) consisting of a cooled charge-coupled device (CCD) camera, a cold cathode discharge tube

and a vacuum chamber at Okayama University of Science, Japan. This was operated with electron beams generated by excitation voltage of 10 kV and beam current of 0.5 mA at vacuum condition, i.e. less than 100 Torr. A magnet was used to control the diameter of electron beam spot at 3 μm size on the sample surface. CL images were converted to digital data using the Nikon imaging system (DS-5Mc).

A SEM-CL system installed at Okayama University of Science, Japan provided the CL spectral measurements for this study. This system contains a SEM (JEOL: JSM-5410LV) combined with a grating monochromator (OXFORD: Mono CL2), having a retractable parabolic mirror coated with aluminum (collecting efficiency of 75 %). The CL was dispersed by a grating monochromator with the following characteristics: 1200 grooves/mm, a focal length of 0.3 mm, F of 4.2, limit of resolution of 0.5 nm, and slit width of 4 mm at the inlet and outlet. CL spectral data in the range 300 – 800 nm wavelength were recorded by a photon counting method using a photomultiplier tube (Hamamatsu: R2228) and converted to digital data. Further details of the CL equipment and analytical procedure can be found in (Kayama et al., 2010). Corrected CL spectra in energy units were deconvoluted into the Gaussian components corresponding to each emission center. Peak Analyzer in OriginPro 8J SR2 was used for the correction and deconvolution of each emission center.

Electron probe microanalyser (EPMA)

Electron probe micro (EPM) analyses of topaz phenocrysts were carried out with a four WDS spectrometer-equipped Cameca SX100 electron microprobe at the Spectrum Centre. Beam current of 10 nA, accelerating voltage of 10 kV and 10 μm spot size were used in order to limit element diffusion. A set of natural minerals, including fluorite, Na-pyroxene, olivine, almandine, diopside, K-feldspar, wollastonite, halite, apatite, hematite and rutile, were used as reference materials. Elements were analyzed for 10 to 30 s on-peak and off-peak. The F Kα line was analyzed on a dedicated spectrometer with a PC1 crystal (2d = 60.946 Å). Detection limits, estimated from counting statistics, were between 200 and 500 ppm for most elements, except Fe (800 ppm) and F (1000 ppm).

Laser ablation inductively-coupled plasma mass spectrometry (LA-ICP-MS)

Trace element compositions of topaz phenocrysts were investigated using a Coherent CompEX solid state, 193 nm laser, and an Agilent 7700 quadrupole mass spectrometer at Curtin University. Ablation was performed at 10 Hz repetition rate, 50 μm spot size and approximately 6 J/cm^2 fluence. During the analyses, 20 seconds of background acquisition were followed by 30 s ablation. Additional lines were measured across the growth textures, using 100 s ablation at 4 μm/s speed, corresponding to traverses ~400 μm long. Thirty elements have been monitored, including Li, Mg, Al, Si, P, Na, K, Ca, Ti, V, Cr, Fe, Ga, Mn, Nb, Ta, W, Sn, La, Ce, Nd, Sm, Gd, Tb, Yb, Lu, Y, Pb, Th, U. Quantification of element concentrations was obtained using glass NIST 610 as reference material and assuming stoichiometric abundance of Al in topaz, which was used as the

element of known concentration, or “internal standard”. Glass BCR-2g was measured as a secondary standard. Additional line scans have been performed across CL textures.For these scans, ablation was performed at 10 Hz repetition rate, 30 μm spot size and 3.5 J/cm^2 fluence, and the sample was moved at 3μ/s for 100 s, resulting in 300 μm long lines.

Raman spectroscopy

In situ, non-destructive Raman analyses of topaz were performed with a confocal laser Raman microscope (WITec alpha300R) at the Department of Geology, University of Johannesburg. The spectral range of the spectrometer is 100–4400 cm^{-1}. Raman spectra were collected using 20 X and 100 X Nikon objectives and a frequency doubled Nd:YAG (532 nm) Ar-ion 20-mW monochromatic, non-polarized laser source. Beam centering and Raman spectra calibration were performed daily before spectral acquisition using a Si standard (111). The laser power was set at approximately 25 mW. Raman spectra were compared with reference spectra from the RRUFF Database (Downs, 2006), and spectra from the literature. Raman maps of portions of crystals have been obtained by collecting consecutive spectra at 1 – 2 μm spacing.

Fourier transform infrared spectroscopy

The Fourier transform infrared spectroscopic (FT-IR) investigation of the selected topaz grains was done by using Nicolet continuμm infrared microscope settled at Okayama University of Science, Okayama, Japan. This instrument contains Köhler illumination for reflection and transmission, 4x, 10x, 20x and 40x

visible objectives as well as wide and mid-band MCT-detectors providing good spectral resolution. The wavenumber range is between from 0 to 4000 cm^{-1}.

Results

CL (SEM-CL panchromatic images, color optical images and spectral measurements)

Panchromatic SEM-CL images of topaz phenocrysts show marked brightness variations, defining euhedral to lobed growth textures. In several cases, CL-bright zones follow, or are followed by truncation of growth textures (Fig 1). A prominent feature in CL images is represented by a rim, up to ~100 – 200 μm wide, which contains abundant quartz inclusions (Fig 1). This rim, particularly well-developed on pyramidal facets rather than prisms, represents a late overgrowth and is separated from crystal cores by a commonly rounded surface truncating growth textures. In several grains, this overgrowth includes a dominantly CL-bright discontinuous layer of topaz, which immediately follows the truncation contact (Fig 1A, 1C, 1E). This CL-bright layer has a smooth internal contact, and a mostly lobed, strongly anhedral external margin. Round quartz inclusions, up to few tens of μm across, are distributed along growth textures in the topaz grain rims. These round quartz inclusions resemble quartz crystals in the groundmass (Fig 1).The cores have strong CL-zoning defining mostly euhedral growth textures and, in some cases, show prominent CL sector zoning (Fig 1C, 1E, cf. Akizuki et al., 1979). CL images taken after exposure to the

electron beam (e.g. after EPMA) show darker areas demonstrating the time-dependent nature of this luminescence (Fig 1E).

Optical CL color images of the topaz crystals exhibit blue emission with variable intensity. Textures defined by these variations match SEM-CL images (Fig 2), although in some cases bright domains in SEM-CL appear as darker in optical images and vice versa. All analyzed CL spectra have a major emission in the near-ultraviolet to visible range (blue emission) with peak at around 393 nm (3.16 eV, Fig 3) and another band at shorter wavelength in the near-ultraviolet region, which extends out of our observation range. The blue emission is broad and has full width at half maximum of ~0.8 eV. This is in agreement with the optical CL images showing intense blue luminescence. Dark and bright domains are characterized by the same peaks and are only distinguished by moderate differences in intensity.

Chemical zoning (EPMA and LA-ICP-MS)

Major and minor element chemical zoning was studied with EPMA traverses across CL zones. Overall, EPMA indicates high contents of F (20.7 – 22.3 wt%, Table 2). The rims, as defined by CL images, are slightly enriched in F compared with the cores (mostly F ≥21.5 wt%, Fig 4). Small amounts of P (up to 0.1 wt%) were measured in the cores, and analyses with P above detection limit (200 ppm) have broad negative correlation with Si. Recalculations based on two Al atoms per formula unit indicate a slight Si deficiency (Si = 0.97 – 0.99 apfu) and slight F excess, even in the cores (cores F = 2.03 – 2.16, rims F = 2.10 – 2.17

238 apfu). Totals are between 99.3 and 101.0 wt%. Although the recalculations
239 suggest total saturation of the OH site by F, totals less than 100 wt% allow the
240 presence of a small amount of water in topaz (OH/(OH+F) ≤0.05, or 5%
241 replacement of F by OH).

242 Trace element contents of topaz phenocrysts have been analyzed along
243 traverses across the growth textures identified by CL images by LA-ICP-MS. The
244 analyses indicate significant compositional variations between growth zones. The
245 phenocryst rims tend to be enriched in several trace elements in comparison with
246 the cores (Fig 4C, 4D). The highest concentrations of trace elements were
247 measured for Ca, Na, Fe, and P, which are present at 10^2 to 10^4 ppm levels.
248 Lithium and Ga are present at ppm to tens of ppm levels. Elements such as Nb,
249 Ta and W are present in variable concentrations, mostly at the 10^{-1} to 10^2 ppm
250 levels. Cores contain average Nb and W concentrations of 1.2 and 1.6 ppm,
251 respectively, compared with 4.5 ppm Nb and 4.3 ppm W in the rims. CL-bright
252 areas tend to have higher concentrations of Li, Nb, Ta, W and Ga (Fig 5), and
253 are positively correlated with each other (Fig 4C, 4D).

254 *Raman spectroscopy*

255 Raman spectra of topaz phenocrysts show, in addition to the well-reported
256 peaks (major peaks at 243, 271, 290, 940 cm^{-1}; Downs, 2006), several
257 secondary peaks of variable intensity at ~337, 365, 407, 462, 526, 644, 857, 992,
258 1014,1020 and 1172 cm^{-1} (Fig 6), which have also been described by Beny and
259 Piriou (1987), Kloprogge and Frost (2000), and Skvortsova et al. (2013). Most of

these peaks have been assigned to various modes of vibration of SiO_4 tetrahedra, AlO_6 octahedra, and Al-F, whereas a few peaks already observed at 243, 526 and 644 cm^{-1} (e.g. Griffith, 1969; Skvortsova et al., 2013) are yet to be interpreted. A broad peak with variable intensity at ~1117 – 1120 cm^{-1} may be due to epoxy contamination. A narrow peak was observed at ~3653 cm^{-1}, corresponding to the OH stretching vibration (Kloprogge and Frost, 2000). In addition, spectra collected in different portions of phenocrysts show variable background. In particular, spectra collected in proximity of the core-rim boundary show intense fluorescence in the medium-high frequency range (>1200 – 1500 cm^{-1}). Raman maps reveal that high background fluorescence is distributed along growth textures corresponding to CL-bright zones, implying a strong textural control (Fig 7).

FTIR

The IR spectra of selected topaz grains (a total of 14 spectra) show almost the same spectral features, which are summarized in Figure 8. In all the analyzed points there is a major absorbance (at around 65%) between 875 and 1100 cm^{-1} (Fig 8, point a). This broad peak is related to the SiO_4 tetrahedral stretching vibrational modes. A weak absorbance is shown in spectral regions from 1500 to 1800 cm^{-1}, as well as from 2250 to 2400 cm^{-1} (Fig. 8, points b and c), which might be related to stretching and bending modes of SiO_4 tetrahedra and $Al(OH,F)_2O_4$ octahedra. In addition, a relatively weak absorbance (around 95%) at around 3750 cm^{-1} is assigned to the OH-stretching mode (Fig 8, point d).

However, the F-OH relationship and its IR properties cannot be interpreted in these topaz samples.

Discussion

Basics of CL emission

CL emission is an optical phenomenon, which produces photon emission in the visible light, near-ultraviolet and near-infrared ranges due to the interaction between a high energy electron beam and a solid surface (e.g., Marfunin, 1979; Yacobi and Holt, 1990; Waychunas 2014 and references therein). As a first approximation, luminescence can be grouped into two types: (a) intrinsic CL, which is induced by vacancies, poor ordering, radiation damage, shock damage, such as structural imperfections characterizing the material; and (2) extrinsic CL, which is created from luminescence centers such as impurities (activators) (Marshall, 1988, Remond et al., 1992). Elements present as impurities can be classified, according to their effect on CL emission, as activators, quenchers or neutral (i.e. not affecting luminescence).

In addition, the luminescence of an ion will depend on the interactions with other components in the mineral lattice, its position in the crystal, and on the crystal field (Burns, 1993; Götze, 2012). If the influence of the crystal field is weak, the resulting luminescence emission is characterized by narrow emission lines, whereas if the electron transitions take place in energy levels that are influenced by the local crystal field, luminescence emission spectra show

303 relatively broad bands (Götze, 2012). As a consequence, the luminescence
304 emission of each activator element varies from mineral to mineral and is specific
305 for the crystal structure of the host crystal (Götze, 2012). Thus, incorporation of
306 trivalent rare earth elements at trace concentrations in quartz results in emissions
307 with characteristic sharp peaks, due to the low level of interaction between the
308 impurity and the host lattice (Götze et al., 2004; Correcher et al., 2011).
309 Incorporation of transition metals in quartz and topaz results in somewhat
310 broader luminescence peaks, since the partially filled 3d electron shells are
311 comparatively less shielded by the external 4s shell (e.g. 2.95 eV emission of Ti
312 in quartz, Muller et al., 2002). In contrast, structural defects cause wide
313 luminescence peaks, due to the high level of interaction with the host mineral
314 (Stevens-Kalceff, 2009)

315 *Major element (F-OH) substitutions and trace element uptake mechanisms of*
316 *topaz*

317 Topaz in magmatic rocks tends to have lower OH/(OH+F) than
318 metamorphic or hydrothermal topaz., OH/(OH+F) replacement up to 0.3 (F 1.4,
319 OH 0.6 apfu, or replacement of F by OH up to 30%) has been measured in
320 hydrothermal deposits (Barton, 1982), and OH/(OH+F) = 0.35 – 0.55 (35 – 55 %
321 F-OH replacement) has been reported from the ultra-high pressure metamorphic
322 Sulu terrane, China (Zhang et al., 2002), whereas topaz from granite in the
323 Krušné Hory/Erzgebirge area has lower OH/(OH+F) of ~ 0.05 (or OH = 0.1 apfu)
324 (Breiter et al., 2013).

EPMA carried out as part of this study indicates high F concentrations, and even an apparent F-oversaturation (a pure F topaz would contain 20.65 wt% F). Fluorine contents higher than this value may be due to an analytical artefact (as F contents may be affected by grain orientation (e.g. Ottolini et al., 2000), although mild analytical conditions (low beam intensity, defocused beam) were used to minimize element diffusion under the electron beam during analysis. Despite the presence of OH, as detected by Raman spectroscopy, the near-pure composition of topaz [$Al_2SiO_4F_2$] measured in this study (OH/(OH+F) ≤0.5) is consistent with a magmatic origin.

Variable concentrations of P (up to 1 wt%), and Fe (31 – 1296 ppm), Ge (26 – 104 ppm), Sc (2 – 12 ppm), Sn (1 – 30 ppm) and Ga (2 – 29 ppm) were measured in topaz from granites in the Krušné Hory/Erzgebirge area (Breiter et al., 2013). Vanadium (occurring as V^{4+}), Mn (as Mn^{3+}), Ti (as Ti^{4+}), Cr (as Cr^{3+}) at tens to hundreds of ppm levels have been detected by EPMA and electric paramagnetic resonance (EPR) in gem-quality topaz from Ouro Preto, Brazil (Schott et al., 2003). Wasim et al. (2011) analyzed a large number of elements by K_0-INAA in topaz from Pakistan, including Mn, Fe and Na at hundreds to tens of thousands ppm levels, As, Br, light REE, Co, Cr, Cs, Ga, Ge, Hf, Rb, Sb, Sc, Th, U, Zn at ppm to tens of ppm levels, and Ta, W and HREE, mostly at sub-ppm levels, although these authors do not specify the origin of these topaz crystals. Hervig et al. (1987) analyzed Li and B in topaz from rhyolites of the North American Cordillera by ion probe, and found that topaz in volcanic rocks has higher Li and B than topaz from hydrothermal and metamorphic environments.

348 The smooth time-resolved LA-ICP-MS signals in our analyses suggest that
349 trace elements are incorporated in the mineral structure, rather than in discrete
350 inclusions. Based on simple charge balance considerations, replacement of Si by
351 other cations in the 4+ oxidation state (e.g. Ti, V, Ge), and replacement of Al^{3+} by
352 3+ cations (Ga, Fe, Mn, REE) seem plausible (e.g. Northrup and Reeder, 1994;
353 Wunder and Marler, 1997; Gatta et al., 2006).

354 Intake of Nb, Ta, P, which usually occur in the 5+ oxidation state, and W (5+
355 or 6+) (Farge et al., 2006), would require coupled substitution. In the
356 peraluminous granites and greisens in the Podlesı granite, central Europe,
357 replacement of (Si^{4+} + Si^{4+}) by (P^{5+} + Al^{3+}) has been proposed (Breiter et al.,
358 2013). A weak negative P – Si correlation in our EPM analyses seems to indicate
359 the same type of substitution (Fig 4B). A similar mechanism may be involved in
360 the replacement of Nb, Ta and W in the 5+ oxidation state (e.g. Si^{4+} + Si^{4+} =
361 $(Nb,Ta,W)^{5+}$ + $(Al,Ga)^{3+}$). In addition, the correlation between these elements and
362 Li may indicate a replacement Al^{3+} + Al^{3+} = $(Nb,Ta,W)^{5+}$ + Li^{1+}.

363 As an additional mechanism for the incorporation of alkalis, it has been
364 proposed that Al^{3+} replaces tetrahedral Si^{4+} in quartz, while monovalent ions (H^+,
365 Li^+, Na^+, K^+), acting as charge compensating ions, are situated in channels
366 parallel to the c-axis (Cohen, 1960).

367 *Cathodoluminescence properties of topaz*

368 In terms of the energy states between conduction and valance bands of the
369 excited electrons in the sample, topaz is a wide band gap insulating mineral

(approximately 10 eV; Priest et al., 1987). This band gap is wide enough to avoid any of the spontaneous thermal ionization processes, which do not emit cathodoluminescence signal. On the other hand, the wide band gap of topaz provides several possibilities for the recombination centers or traps of the excited electrons.

Correcher et al. (2011) have identified a CL and thermoluminescence emission in the blue region (480 nm) of the spectrum of natural topaz at low temperature, and a minor emission in the red region (650 – 700 nm). These authors noted a strong dependence of both emissions on temperature, and attributed the low frequency (red) emission to impurities, and the high-frequency (blue) emission to structure defects. Gaft (2005) reported a laser-induced blue emission in natural topaz centered at 455 nm, and attributed it to the presence of Ti. These emissions are higher than the main emission found in our study, although the correction made on our measurements could be at least in part responsible for this difference (e.g. Kayama et al., 2010).

We interpret the emission center at 393 nm in the blue region of the electromagnetic spectrum of topaz found in this study as being due to intrinsic luminescence centers, which should be assigned to point defects. The recombination centers occur close to the conduction band providing relatively low wavelength emission at around the near UV range such as the one observed here. According to Remond et al. (2000), broad featureless CL spectra are generally related to point defect centers including vacancies as well as interstitial clusters.

393 Priest et al. (1987) identified diamagnetic point defect centers by electron
394 spin resonance (ESR) spectroscopy in topaz, where the defect is an interstitial
395 oxygen atom in the form of a peroxy radical (=Si-O-O). Priest et al. (1991)
396 observed blue luminescence during electron bombardment of topaz, and
397 tentatively attributed this emission to the peroxy radicals. More recently,
398 Correcher et al. (2011) analyzed topaz samples from Badajoz (Spain) at low
399 temperature; they described defect-related bands in the blue region of the
400 electromagnetic spectrum, which they attributed to the $(AlO_4)o$ and $(H_3O_4)o$
401 centers. These mechanisms are possible in our samples, although they cannot
402 be ascertained, based on our dataset.

403 Alternatively, the major and trace element replacement may be responsible
404 for the formation of point defect centers. The replacement of OH for F is known to
405 affect the optical and structural properties of topaz, and cell parameters *a* and *b*
406 have a negative linear correlation with the F concentration that results in
407 geometry change (from space group Pbnm to $Pbn2_1$) at F replacement >50%
408 (Wunder et al., 1993; Zhang et al., 2002; Alberico et al., 2003; Schott et al.,
409 2003), thus potentially affecting the luminescence properties. Expected changes
410 of luminescence properties may include wavelength shift, changes in emission
411 band width and peak appearance or disappearance, and changes in the
412 emission mechanisms may be induced by the way this substitution modifies the
413 effect of the activator or defect responsible for emission. However, no clear
414 correlation was found between total F content in EPM analyses and CL intensity
415 in the samples we studied. This suggests that the replacement of F for OH does

not affect CL emission in our samples. It is also worth noting that our samples have high F contents (F ≥ 20.7 wt%), which would result in minor structural changes, according to Alberico et al. (2003), and that an effect oc CL at higher degrees of F-OH replacement cannot be ruled out.

The incorporation of trace elements can induce a distortion of the mineral lattice that may cause CL emission. Because of the very similar ionic radii, replacement of Si^{4+} by P^{5+} (54 pm against 52 pm, respectively) would not cause a large lattice distortion. However, substitution of Ga^{3+} (ionic radius 76 pm) for Al^{3+} (68 pm), and Nb^{5+} and Ta^{5+} (78 pm) for Si^{4+} (54 pm) would imply much more significant lattice distortion. For example, in high-temperature (magmatic) α-quartz, the replacement of Ti^{4+} (ionic radius 74 pm) for Si^{4+} is interpreted to have a role in the blue CL emission (Müller et al., 2000; Krambrock et al., 2007). The correlation found between trace element contents (especially Li, Nb, Ta and W) and CL suggests that a similar mechanism may be involved in our samples. In addition, the altervalent substitution will have a strong influence on the local electronic structure of the crystal structure, thus potentially affecting CL emission. Altervalent replacement of cations can bond excited electrons, thus forming a trap (Waychunas, 2014). In quartz, a CL emission at ~380 -390 nm has been attributed to [AlO_4/M^+] centers, where M^+ can be Li^+, Na^+ or H^+, an altervalent substitution that entails replacement of Si by Al in the tetrahedra and a monovalent cation to balance the charge (e.g. Alonso et al., 1983; Perny et al., 1992; Götze et al., 2001; Kayama et al., 2009).

The interplay between petrological processes and CL

The rims of topaz phenocrysts overgrew an anhedral, round surface that truncates growth textures in the cores, suggesting a resorption event followed by further crystal growth. The phenocryst rims have very bright CL anhedral zones associated with high trace element concentrations, especially Nb, Ta, W, and Li (Fig 1, 2, 5). These domains also have characteristic Raman response, with very high background (Fig 7). It is known that fast crystal growth enhances the non-equilibrium uptake of trace elements and typically results in anhedral growth textures (e.g. Watt et al., 1997; Gabitov et al., 2008), and the accumulation of lattice defects. In our samples, the intense CL and "anomalous" Raman properties described above may have been caused by such processes of rapid growth and lattice defect accumulation. The entrapment of fine grained quartz crystals (Fig 1) suggests that the rims grew together with the groundmass, which typically forms at high levels of undercooling (supersaturation) and nucleation rate, possibly as a consequence of magma eruption, or emplacement at shallow crustal levels.

Implications

The textures and chemical zoning of topaz record valuable information on the evolution of F-rich magmas. However, in order to use the CL of topaz as a reliable petrological indicator, its properties (e.g. trace element dependence) must be better understood. In our study, we found that SEM-CL images of magmatic topaz indicate domains with varying emission, indicating episodes of crystal growth and resorption. Color CL images and CL spectra indicate that CL-

461 dark and –bright areas are both characterized by blue emission, and have a
462 broad peak in the near-ultraviolet to visible range centered at 393 nm. Elements
463 such as Cr^{3+}, Mn^{3+}, V^{4+}, which have previously been indicated to cause CL in
464 topaz (Gaft, 1998, 2005) have not been found to be effective CL activators in our
465 samples. Instead, comparison between CL images and trace element
466 concentrations obtained by EPMA and LA-ICP-MS indicates a correlation
467 between the concentrations of Nb, Ta W, Li and Ga and CL intensity. Further, CL
468 emission is highest in discontinuous rims characterized by high trace element
469 contents (Nb, Ta, W, Li, Ga, REE) and high background in Raman spectra.

470 Although we could not unambiguously assign the CL peaks to specific
471 emission centers in our samples, it is likely that the substitution of trace elements
472 in the structure of topaz caused point defect centers in the form of a lattice
473 distortion and altervalent replacement that caused luminescence. This
474 hypothesis is supported by the correlation between Nb, Ta, W, Li and Ga with CL
475 intensity in our samples (Fig 5). Based on similar CL emissions in quartz, ther
476 intrinsic point defect centers, such as peroxy radicals, are additional possible
477 mechanisms for the CL observed in our samples. Our results suggest that the
478 intake of impurities, with consequent distortion of the mineral lattice and
479 modification of the local electronic structure, may be responsible for increase of
480 CL intensity of topaz. More studies, such as electron energy loss spectrometry
481 (EELS) as well as electron spin resonance (ESR) are necessary to fully
482 understand the nature of trace element uptake and the controls on CL emission
483 of topaz, which remain largely unknown (MacRae and Wilson 2008).

Acknowledgments

This research was supported by a Post-Doctoral Fellowship of the National Research Foundation of South Africa and a Post-Doctoral Fellowship of Curtin University to AA. N. Vladykin is thanked for providing sample material for this study. Christian Reinke (UJ) and Bradley McDonald (Curtin) are thanked for analytical assistance on the EPMA and LA-ICP-MS. The authors are thankful to Masahiro Kayama (Kobe University, Japan) for his useful comments and literature suggestions to this manuscript.

References

Agangi, A., Kamenetsky, V.S., Hofmann, A., Przybyłowicz, W., and Vladykin, N.V. (2014) Crystallisation of magmatic topaz and implications for Nb–Ta–W mineralisation in F-rich silicic melts — The Ary-Bulak ongonite massif. *Lithos*, **202–203**, 317-330.

Agangi, A., McPhie, J., and Kamenetsky, V.S. (2011) Magma chamber dynamics in a silicic LIP revealed by quartz: The Mesoproterozoic Gawler Range Volcanics. *Lithos*, **126**, 68-83.

Akizuki, M., Hampar, M.S., and Zussman, J. (1979) An explanation of anomalous optical properties of topaz. Mineralogical Magazine, **43**, 237-241.

Alberico, A., Ferrando, S., Ivaldi, G., and Ferraris, G. (2003) X-ray single-crystal structure refinement of an OH-rich topaz from Sulu UHP terrane (Eastern China) – Structural foundation of the correlation between cell parameters and fluorine content. *European Journal of Mineralogy*, **15**, 875-881.

506 Alonso, P.J., Halliburton, L.E., Kohnke, and E.E. & Bossoli, R.B. (1983) X-ray
507 induced luminescence in crystalline SiO_2. J Applied Physics, **54**, 5369–
508 5375.
509 Antipin, V.S., Andreeva, I.A., Kovalenko, V.I., and Kuznetsov, V.A. (2009)
510 Geochemical specifics of ongonites in the Ary-Bulak Massif, eastern
511 Transbaikalia. *Petrology*, **17**, 558-569.
512 Badanina, E.V., Trumbull, R.B., Dulski, P., Wiedenbeck, M., Veksler, I.V., and
513 Syritso, L.F. (2006) The behavior of rare-earth and lithophile traace
514 elements in rare-metal granites: a study of fluorite, melt inclusions and
515 host rocks from the Khangilay Complex, Transbaikalia, Russia. *The*
516 *Canadian Mineralogist*, **44**, 667-692.
517 Barton, M.D. (1982) The thermodynamic properties of topaz solid solutions and
518 some petrologic applications. *American Mineralogist*, **67**, 956-974.
519 Bastos Neto, A.C., Ferron, J.T.M.M., Chauvet, A., Chemale Jr, F., de Lima, E.F.,
520 Barbanson, L., and Costa, C.F.M. (2014) U–Pb dating of the Madeira
521 Suite and structural control of the albite-enriched granite at Pitinga
522 (Amazonia, Brazil): Evolution of the A-type magmatism and implications
523 for the genesis of the Madeira Sn–Ta–Nb (REE, cryolite) world-class
524 deposit. *Precambrian Research*, **243**, 181-196.
525 Beny, J.M., and Piriou, B. (1987) Vibrational spectra of single-crystal topaz.
526 *Physics and Chemistry of Minerals*, **15**, 148-159.
527 Bradley, D., and McCauley, A. (2013) A Preliminary Deposit Model for Lithium-
528 Cesium-Tantalum (LCT) Pegmatites, Open-File Report 2013–1008, p. 7.

529 Breiter, K.M. (2009) Evolution of rare-metal granitic magmas documented by
530 quartz chemistry. *European Journal of Mineralogy*, **21**, 335-346.
531 Breiter, K.M., Gardenová, N., Vaculovič, T., and Kanický, V. (2013) Topaz as an
532 important host for Ge in granites and greisens. *Mineralogical Magazine*,
533 **77**, 403-417.
534 Burt, D.M., Sheridan, M.F., Bikun, J.V., and Christiansen, E.H. (1982) Topaz
535 rhyolites; distribution, origin, and significance for exploration. *Economic*
536 *Geology*, **77**, 1818-1836.
537 Charoy, B., and Noronha, F. (1996) Multistage growth of a rare-element, volatile-
538 rich microgranite at argemela (Portugal). *Journal of Petrology*, **37**, 73-94.
539 Cohen, A.J. (1960) Substitutional and interstitial aluminum impurity in quartz,
540 structure and color center interrelationships. *Journal of Physics and*
541 *Chemistry of Solids*, **13**, 321-325.
542 Congdon, R.D., and Nash, W.P. (1988) High-fluorine rhyolite: An eruptive
543 pegmatite magma at the Honeycomb Hills, Utah. *Geology*, **16**, 1018-1021.
544 Correcher, V., Garcia-Guinea, J., Martin-Fernandez, C., and Can, N. (2011)
545 Thermal effect on the cathodo- and thermoluminescence emission of
546 natural topaz ($Al_2SiO_4(F,OH)_2$). *Spectroscopy Letters*, **44**, 486-489.
547 da Silva, N.D., Guedes, K.J., Pinheiro, M. V.B., Schweizer, S., Spaeth, J-M., and
548 Krambrock, K. (2005) The O-(Al_2) centre in topaz and its relation to the
549 blue colour. *Physica Status Solidi C*, **2**, 397-400.
550 Downs, R.T. (2006). The RRUFF Project: an integrated study of the chemistry,
551 crystallography, Raman and infrared spectroscopy of minerals. Program

552 and Abstracts of the, 19th General Meeting of the International
553 Mineralogical Association in Kobe, Japan, pp. 03–13.
554 Farges, F., Linnen, R.L., and Brown, G.E. (2006) Redox and speciation of tin in
555 hydrous silicate glasses: a comparison with Nb, Ta, Mo and W. *The*
556 *Canadian Mineralogist*, **44**, 795-810.
557 Fukumi, K., and Sakka, S. (1988) Coordination state of Nb5+ ions in silicate and
558 gallate glasses as studied by Raman spectroscopy. Journal of Materials
559 Science, **23**, 2819-2823.
560 Gabitov, R.I., Gaetani, G.A., Watson, E.B., Cohen, A.L., and Ehrlich, H.L. (2008)
561 Experimental determination of growth rate effect on U^{6+} and Mg^{2+}
562 partitioning between aragonite and fluid at elevated U^{6+} concentration.
563 *Geochimica et Cosmochimica Acta*, **72**, 4058-4068.
564 Gaft, M., Reisfeld, R., and Panczer, G. (2005) Modern luminescence
565 spectroscopy of minerals and materials. 356 p. Springer-Verlag,
566 Heidelberg.
567 Gaft, M., Reisfeld, R., Panczer, G., Blank, P., and Boulon, G. (1998) Laser-
568 induced time-resolved luminescence of minerals. Spectrochimica Acta
569 Part A: *Molecular and Biomolecular Spectroscopy*, **54**, 2163-2175.
570 Gatta, G.D., Nestola, F., Bromiley, G.D., and Loose, A. (2006) New insight into
571 crystal chemistry of topaz: A multi-methodological study. American
572 Mineralogist, **91**, 1839-1846.

573 Götze, J. (2012) Application of cathodoluminescence microscopy and
574 spectroscopy in geosciences. *Microscopy and Microanalysis*, **18**, 1270-
575 1284.
576 Götze, J., Plötze, M., Graupner,T., Hallbauer, D.K. and Bray, C.J. (2004) Trace
577 element incorporation into quartz: A combined study by ICP-MS, electron
578 spin resonance, cathodoluminescence, capillary ion analysis, and gas
579 chromatography. Geochimica et Cosmochimica Acta, **68**, 3741 - _3759.
580 Götze, J., Plötze, M., and Habermann, D. (2001) Origin, spectral characteristics
581 and practical applications of the cathodoluminescence (CL) of quartz – a
582 review. *Mineralogy and Petrology*, **71**, 225-250.
583 Griffith, W.P. (1969) Raman studies on rock-forming minerals. Part I.
584 Orthosilicates and cyclosilicates. *Journal of the Chemical Society A:*
585 *Inorganic, Physical, Theoretical*, 1372-1377.
586 Gucsik, A. (2009) Cathodoluminescence and its application in the planetary
587 sciences. 160 p. Springer-Verlag Heidelberg.
588 Hayward, C.L. (1988) Cathodoluminescence of ore and gangue minerals and its
589 application in the minerals industry. In L.J. Cabri, and D.J. Vaughan, Eds.
590 *Modern Approaches to Ore and Environmental Mineralogy*, **27**, 269-325.
591 Hervig, R.L., Kortemeier, W.T., and Burt, D.M. (1987) Ion-microprobe analyses of
592 Li and B in topaz from different environments. *American Mineralogist*, **72**,
593 392-396.

Kayama, M., Nakano, S., and Nishido, H. (2010) Characteristics of emission centers in alkali feldspar: A new approach by using cathodoluminescence spectral deconvolution. *American Mineralogist*, **95**, 1783-1795.

Kloprogge, J.T., and Frost, R.L. (2000) Raman microscopic study at 300 and 77 K of some pegmatite minerals from the Iveland–Evje area, Aust-Agder, Southern Norway. *Spectrochimica Acta Part A: Molecular and Biomolecular Spectroscopy*, **56**, 501-513.

Kostitsyn, Y.A., Kovalenko, V.I., and Yarmolyuk, V.V. (1996) Rubidium-strontium isochron for the Arybulak ongonite stock, eastern Transbaikalia. Transactions (Doklady) of the Russian Academy of Sciences. Earth science sections.

Kovalenko, V.I., and Kovalenko, N.I. (1976) Ongonites (topaz bearing quartz keratophyre)-subvolcanic analogue of rare metal Li-F granite. Nauka Press.

Krambrock, K., Ribeiro, L.G.M., Pinheiro, M.V.B., Leal, A.S., de C.B. Menezes, M.Â., Spaeth J.-M (2007) Color centers in topaz: comparison between neutron and gamma irradiation. *Physics and Chemistry of Minerals*, **34**, 437-444.

London, D., and Kontak, D.J. (2012) Granitic pegmatites: scientific wonders and economic bonanzas. *Elements*, **8**, 257-261.

MacRae, C.M., and Wilson, N.C. (2008) Luminescence database I - Minerals and materials. *Microscopy and Microanalysis*, **14**, 184-204.

Manning, D.A.C., and Hill, P.I. (1990) The petrogenetic and metallogenic significance of topaz granite from the southwest England orefield. In H.J. Stein, and J.L. Hannah, Eds. *Ore-bearing granite systems; Petrogenesis and mineralizing processes*, **246**. Geological Society of America.

Marfunin, A.S. (1979) Spectroscopy, luminescence and radiation centers in minerals. Springer, Berlin, Heidelberg, New York.

Marshall, D.J. (1988) Cathodoluminescence of geological materials. Unwin Hyman, Boston.

Müller, A., Lennox, P., and Trzebski, R. (2002) Cathodoluminescence and micro-structural evidence for crystallisation and deformation processes of granites in the Eastern Lachlan Fold Belt (SE Australia). *Contributions to Mineralogy and Petrology*, **143**, 510-524.

Müller, A., Seltmann, R., and Behr, H.J. (2000) Application of cathodoluminescence to magmatic quartz in a tin granite - case study from the Schellerhau Granite Complex, Eastern Erzgebirge, Germany. *Mineralium Deposita*, **35**, 169-189.

Northrup, P.A., and Reeder, R.J. (1994) Evidence for the importance of growth-surface structure to trace element incorporation in topaz. American Mineralogist, **79**, 1167-1175.

Ottolini, L., Cámara, F., and Bigi, S. (2000) An investigation of matrix effects in the analysis of fluorine in humite-group minerals by EMPA, SIMS, and SREF. *American Mineralogist*, **85**, 89-102.

638 Pagel, M., Barbin, V., Blanc, P., and Ohnenstetter, D. (2000)
639 Cathodoluminescence in geosciences. Springer-Verlag, Heidelberg.
640 Payette, C., and Martin, R.F. (1990) Melt inclusions in the quartz phenocrysts of
641 rhyolites from Topaz and Keg Mountains, Thomas Range, Utah.
642 *Geological Society of America Special Papers*, **246**, 89-102.
643 Peretyazhko, I.S., and Savina, E.A. (2010a) Fluid and magmatic processes in the
644 formation of the Ary-Bulak ongonite massif (eastern Transbaikalia).
645 *Russian Geology and Geophysics*, **51**, 1110-1125.
646 Peretyazhko, I.S., and Savina, E.A. (2010b) Sinks of liquid immiscibility in
647 ongonitic magma: Evidence from the study of melt and fluid inclusions in
648 rocks of the Ary-Bulak massif (Eastern Transbaikalia). *Doklady Earth*
649 *Sciences*, **433** (2 DO - 10.1134/S1028334X10080192), 1077-1082.
650 Peretyazhko, I.S., Savina, E.A., Dril', S.I., and Gerasimov, N.S. (2011) Rb–Sr
651 isotope system and Rb–Sr partitioning in the rocks of the Ary-Bulak
652 ongonite massif, formed with the participation of fluoride–silicate magmatic
653 immiscibility. *Russian Geology and Geophysics*, **52**, 1401-1411.
654 Peretyazhko, I.S., Zagorsky, V.Y., Tsareva, E.A., and Sapozhnikov, A.N. (2007)
655 Immiscibility of calcium fluoride and aluminosilicate melts in ongonite from
656 the Ary-Bulak intrusion, Eastern Transbaikal region. *Doklady Earth*
657 *Sciences*, **413** (1 DO - 10.1134/S1028334X07020419), 315-320.
658 Perny B,, Eberhardt P,, Ramseyer K,, Mullis J,, and Pankrath R (1992)
659 Microdistribution of Al, Li, and Na in alpha-quartz - Possible causes and

660 correlation with short-lived cathodoluminescence. American Mineralogist,
661 **77**, 534-544
662 Priest, V., Cowan, D.L., Ros, F.K., and Reichl, D.G. (1987) Point defects in topaz
663 crystals. *Applied Physics Communications*, **7**, 86.
664 Raimbault, L., Cuney, M., Azencott, C., Duthou, J.-L., and Joron, J.L. (1995)
665 Geochemical evidence for a multistage magmatic genesis of Ta-Sn-Li
666 mineralization in the granite at Beauvoir, French Massif Central.,
667 *Economic Geology*, **90**, 548-576.
668 Raw Materials Supply Group, 2014, Critical raw materials for the EU – Report of
669 the Ad-hoc Working Group on defining critical raw materials: Raw
670 Materials Supply Group, European Commission, Enterprise and Industry,
671 41 p. http://ec.europa.eu/enterprise/policies/raw-materials/files/docs/crm-
672 report-on-critical-raw-materials_en.pdf (on line, accessed Dec 2014)
673 Remond, G., Cesbron, F., Chapoulie, R., Ohnenstetter, D., Rouques-Carmes, C.,
674 and Schvoerer, M. (1992) Cathodoluminescence applied to the
675 microcharacterization of mineral materials: a present status in
676 experimentation and interpretation. *Scanning Microscopy*, **6**, 23-69.
677 Remond, G., Phillips, R.M. and Roques-Carmes, C. (2000) Importance of
678 instrumental and experimental factors on the interpretation of
679 cathodoluminescence data from wide band gap materials. In:
680 Cathodoluminescence in geosciences. Springer-Verlag, Heidelberg. p.59-
681 126.

682 Schott, S., Rager, H., Schürmann, K., and Taran, M. (2003) Spectroscopic study
683 of natural gem quality “Imperial” topazes from Ouro Preto, Brazil.
684 *European Journal of Mineralogy*, **15**, 701-706.
685 Skvortsova, V., Mironova-Ulmane, N., Trinkler, L., and Chikvaidze, G. (2013)
686 Optical properties of natural topaz. IOP Conference Series: *Materials*
687 *Science and Engineering*, **49**, 012051.
688 Song, Y., and Yuan, X. (2009) New method for identification of blue topaz - An
689 application of cathodoluminescence (CL). *Journal of Geography and*
690 *Geology*, **1**, 13-19.
691 Stevens-Kalceff, M.A. (2009) Cathodoluminescence microcharacterization of
692 point defects in α-quartz. Mineralogical Magazine, **73**,: 585-605.
693 Syritso, L.F., Badanina, E.V., Abushkevich, V.S., Volkova, E.V., and Shuklina,
694 E.V. (2012) Volcanoplutonic association of felsic rocks in the rare-metal
695 ore units of Transbaikalia: Geochemistry of rocks and melts, age, and P-T
696 conditions of their crystallization. *Petrology*, **20**, 567-592.
697 Taylor, R.P. (1992) Petrological and geochemical characteristics of the Pleasant
698 Ridge zinnwaldite-topaz granite, southern New Brunswick, and
699 comparisons with other topaz-bearing felsic rocks. *The Canadian*
700 *Mineralogist*, **30**, 895-921.
701 Thomas, R. (1982) Ergebnisse der thermobarogeochemischen Untersuchungen
702 an Flüssigkeitseinschlüssen in Mineralen der postmagmatischen Zinn–
703 Wolfram–Mineralisation des Erzgebirges. Freiberg Forsch H C, **370**, 1-85.

Thomas, R., and Davidson, P. (2013) The missing link between granites and granitic pegmatites. *Journal of Geosciences*, **58**, 183-200.

Thomas, R., Davidson, P., Rhede, D., and Leh, M. (2009) The miarolitic pegmatites from the Konigshain: a contribution to understanding the genesis of pegmatites. *Contributions to Mineralogy and Petrology*, **157**, 505-523.

Thomas, R., Webster, J.D., and Heinrich, W. (2000) Melt inclusions in pegmatite quartz: complete miscibility between silicate melts and hydrous fluids at low pressure. *Contributions to Mineralogy and Petrology*, **139**, 394-401.

Thomas, S.-M., Thomas, R., Davidson, P., Reichart, P., Koch-Müller, M., and Dollinger, G. (2008) Application of Raman spectroscopy to quantify trace water concentrations in glasses and garnets. *American Mineralogist*, **93**, 1550-1557.

U.S. Geological Survey, 2011, Mineral commodity summaries 2011: U.S. Geological Survey, 198 p. http://minerals.usgs.gov/minerals/pubs/mcs/2011/mcs2011.pdf (on line, accessed Dec 2014)

Vasyukova, O.V., Goemann, K., Kamenetsky, V.S., MacRae, C.M., and Wilson, N.C. (2013) Cathodoluminescence properties of quartz eyes from porphyry-type deposits: Implications for the origin of quartz. *American Mineralogist*, **98**, 98-109.

Wasim, M., Zafar, W., Tufail, M., Arif, M., Daud, M., and Ahmad, A. (2011) Elemental analysis of topaz from northern areas of Pakistan and

assessment of induced radioactivity level after neutron irradiation for color induction. Journal of *Radioanalytical & Nuclear Chemistry*, **287**, 821-826.

Watt, G.R., Wright, P., Galloway, S., and McLean, C. (1997) Cathodoluminescence and trace element zoning in quartz phenocrysts and xenocrysts. *Geochimica et Cosmochimica Acta*, **61**, 4337-4348.

Waychunas, G.A. (2014) Luminescence spectroscopy. *Reviews in Mineralogy and Geochemistry*, **78**, 175-217.

Williams, P.M., and Yoffe, A.D., 1969. Monochromatic cathodoluminescence image in the scanning electron microscope. Nature, **221**, 952-953.

Williams-Jones, A.E., Samson, I.M., and Olivo, G.R. (2000) The genesis of hydrothermal fluorite-REE deposits in the Gallinas Mountains, New Mexico. *Economic Geology*, **95**, 327-341.

Wunder, B., and Marler, B. (1997) Ge-analogues of aluminum silicates; high-pressure synthesis and properties of orthorhombic $Al_2\ GeO_4(OH)_2$. *European Journal of Mineralogy*, **9**, 1147-1158.

Wunder, B., Rubie, D.C., Ross, C.R., Medenbach, O., Seifert, F., Schreyer, W. (1993) Synthesis, stability, and properties of $Al_2SiO_4(OH)_2$; a fully dehydrated analogue of topaz. *American Mineralogist*, **78**, 285-297.

Yacobi, B.G., and Holt, D.B. (1990) Cathodoluminescence microscopy of inorganic solids. 292 p. Plenum Press, New York.

Zhang J., Lu T., Wang M., Chen H. (2011) The radioactive decay pattern of blue topaz treated by neutron irradiation. *Gems and Gemology*, **47**, 302-307.

749 Zhang, R.Y., Liou, J.G., and Shu, J.F. (2002) Hydroxyl-rich topaz in high-
750 pressure and ultrahigh-pressure kyanite quartzites, with retrograde
751 woodhouseite, from the Sulu terrane, eastern China. *American*
752 *Mineralogist*, **87**, 445-453.
753

Figure captions

Fig. 1. SEM-CL (A, C, E), and SEM-BSE (B, D, F) images of topaz phenocrysts. Arrows indicate truncation of growth textures; dashed lines indicate position of some quartz inclusions. Dark spots in E caused by ca. 10 min exposure to electron beam during EPMA. Abbreviations: Qtz quartz, Toz topaz

Fig. 2. Comparison of parallel polarized transmitted light image (A), SEM-BSE (B), SEM-CL (C) and optical CL (D) of topaz. Abbreviations: Qtz quartz, Toz topaz, Ab albite, Kfs K-feldspar, cb carbonate.

Fig. 3. CL spectra of topaz collected in CL-bright and dark areas. Inset shows the location of CL spectral measurements on optical CL image

Fig. 4. Chemical composition of topaz phenocrysts. Major elements (A, B, analyzed by EPMA) as wt%, trace elements (C, D, analyzed by LA-ICP-MS) as ppm. Note logarithmic scale in C and D. Crystal cores and rims are distinguished. Previous analyses reported in Agangi et al. (2014)

Fig. 5. CL image (**A**) and LA-ICP-MS analyses (**B**, spot analyses, **C**, line scan). Brighter CL domains are associated with higher Nb, Ta, W and Li concentrations. Note trace element increase at the core-rim boundary in B

Fig. 6. Example of a Raman spectrum of topaz. The spectrum was acquired in a section almost parallel to the c axis. Peak assignments (Beny and Piriou, 1987, Fukumi and Sakka, 1988, Kloprogge and Frost 2000, Wunder and Marler, 1997, Skvortsova et al., 2013 and references therein): * various modes of vibration of

775 SiO_4, ° stretching and bending modes of [AlO_6] octahedra coupled with the
776 bending modes of [SiO_4] tetrahedra, □ δ(Al-OH) or OH in-plane bending, □
777 stretching of Al-F (?), e epoxy contamination (?). Non assigned peaks are
778 indicated in bold italic font

779 **Fig. 7.** Parallel polarized transmitted light image (A), SEM-CL image (B) Raman
780 map (C) and Raman spectra (D) of a topaz phenocryst. Raman map has been
781 built by filtering the signal between 3200 and 3800 cm^{-1} (broad background, D).
782 Note the correspondence between very high CL intensity and high Raman
783 background

784 **Fig. 8.** Example of FTIR spectrum

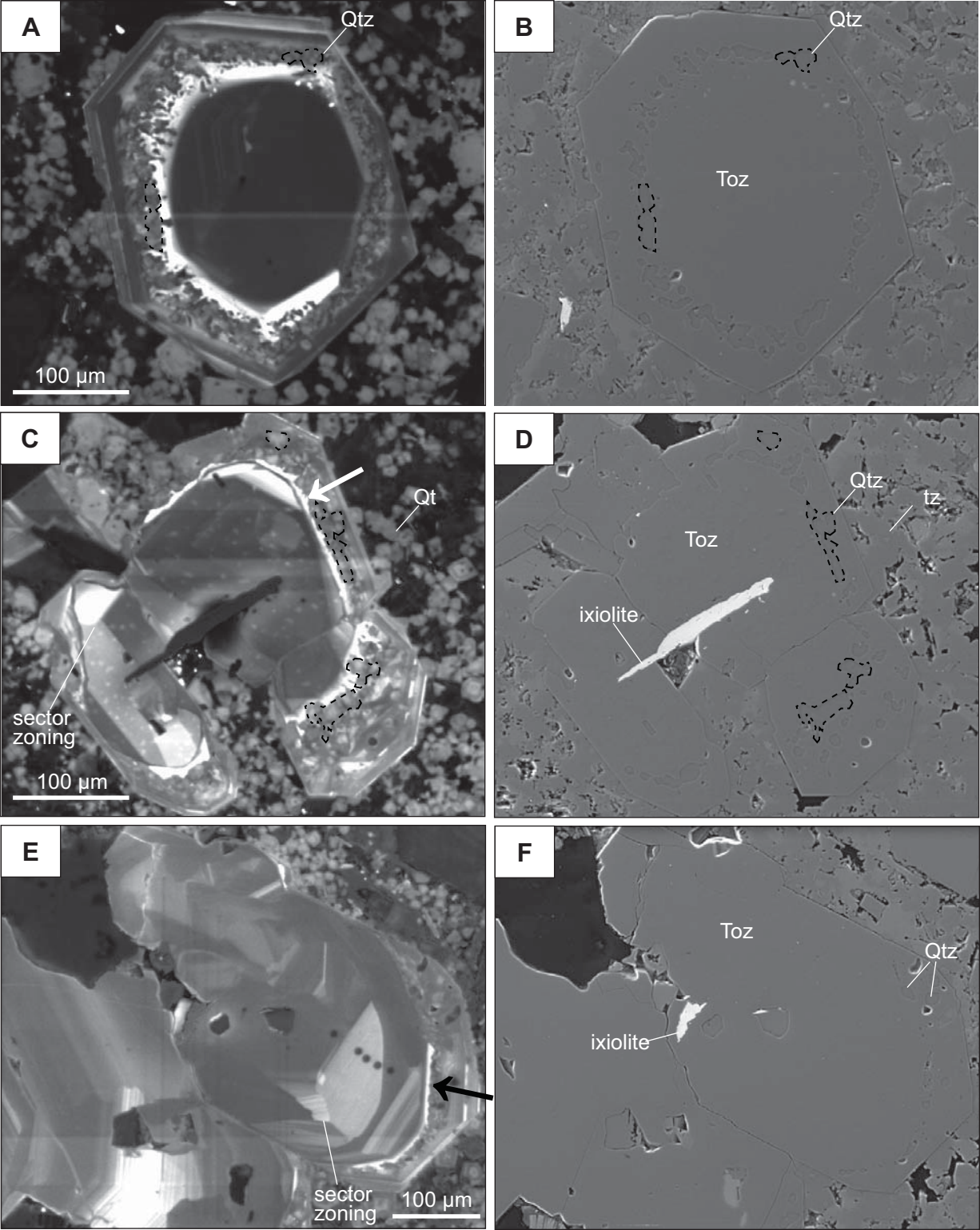
A
Qtz
100 µm
B
Qtz
Toz
C
Qt
sector
zoning
100 µm
D
Qtz
tz
Toz
ixiolite
E
sector
zoning
100 µm
F
Toz
Qtz
ixiolite

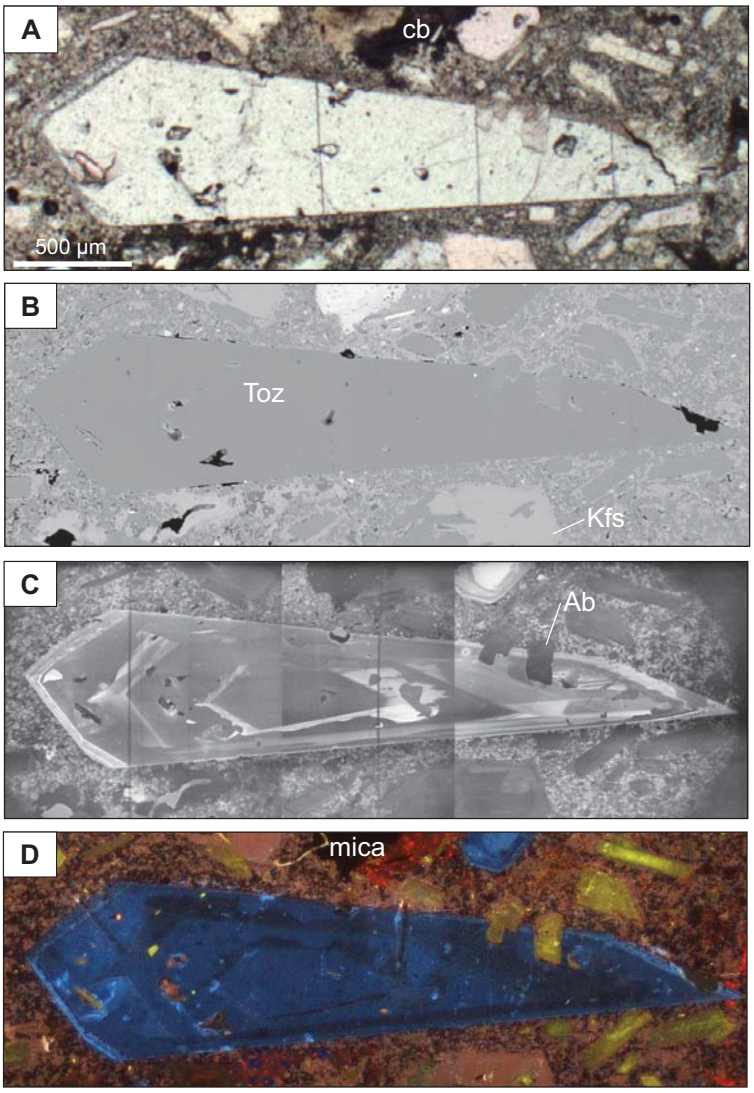
A
cb
500 µm
B
Toz
Kfs
C
Ab
D
mica

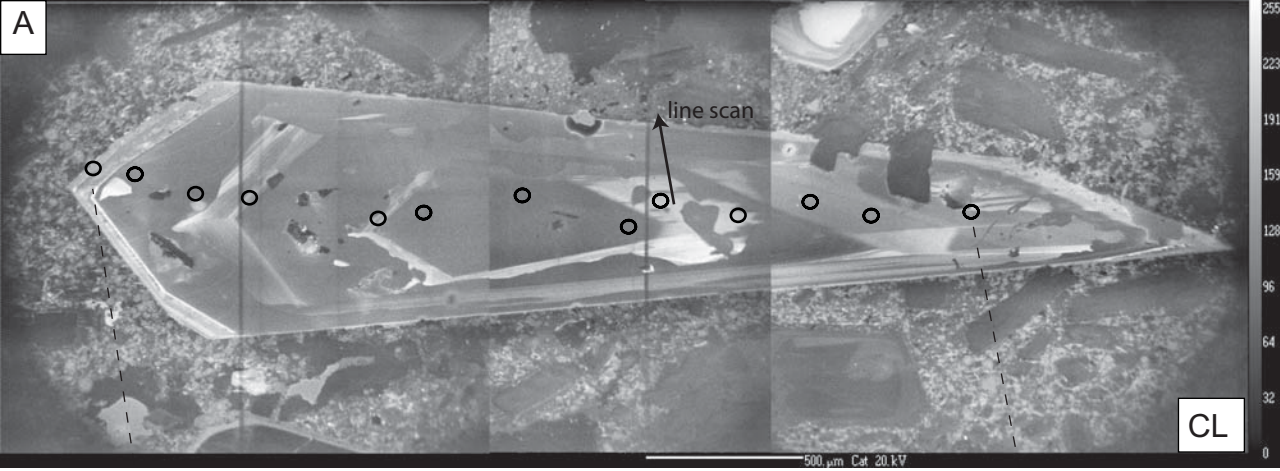
A
line scan
CL
500 µm Cat 20.kV

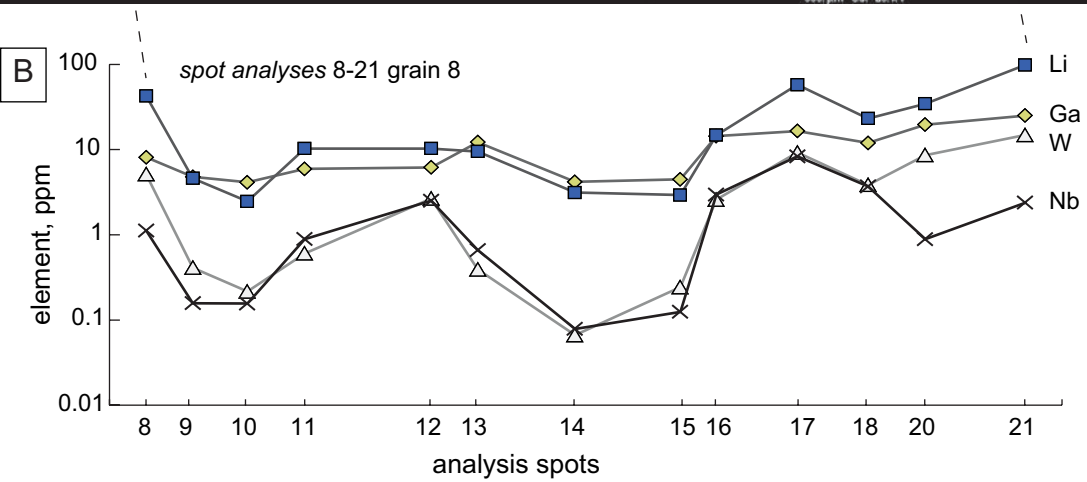
B
spot analyses 8-21 grain 8
element, ppm
100
10
1
0.1
0.01
Li
Ga
W
Nb
8
9
10
11
12
13
14
15
16
17
18
20
21
analysis spots

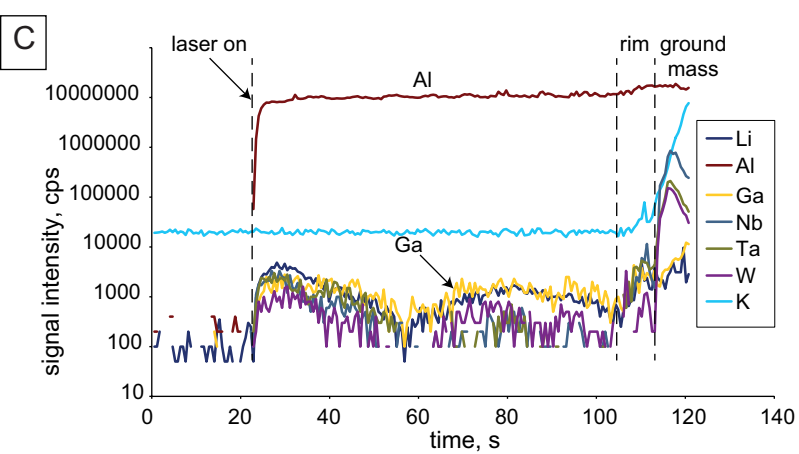
C
laser on
Al
rim
ground mass
Ga
signal intensity, cps
10000000
1000000
100000
10000
1000
100
10
Li
Al
Ga
Nb
Ta
W
K
0
20
40
60
80
100
120
140
time, s

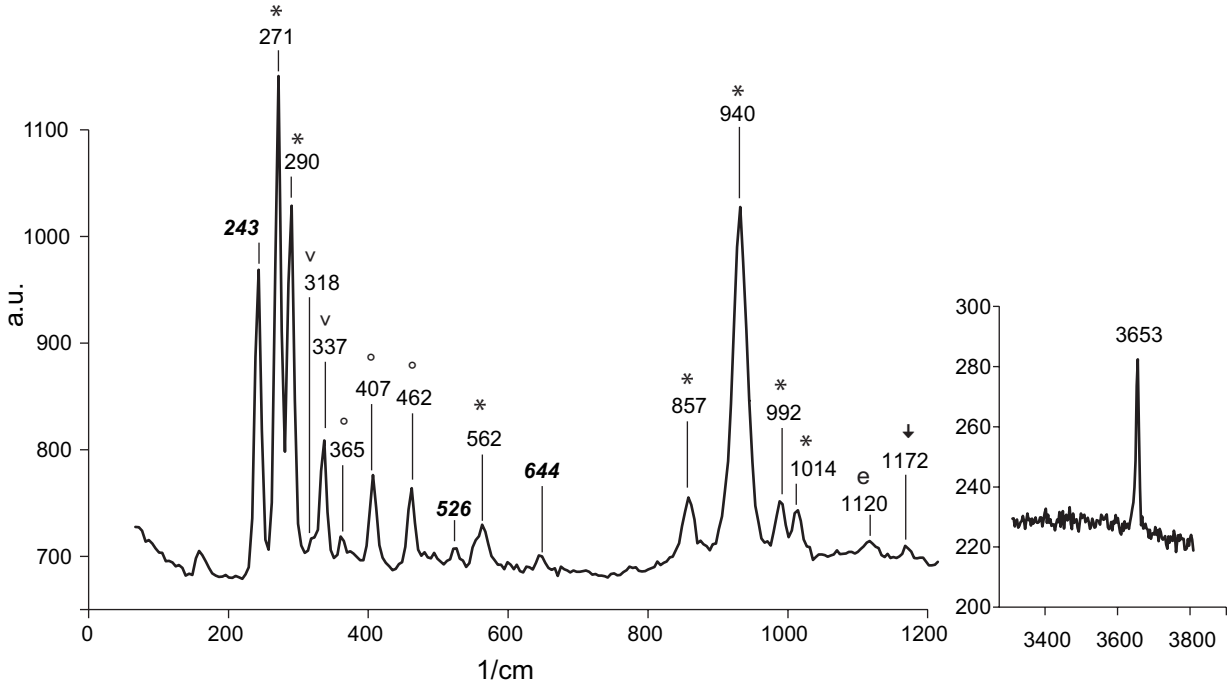
*
271
*
290
243
v
318
v
337
o
407
o
462
o
365
*
562
526
644
*
857
*
940
*
992
*
1014
e
1120
↓
1172
1100
1000
900
800
700
a.u.
0
200
400
600
800
1000
1200
1/cm
300
280
260
240
220
200
3653
3400
3600
3800

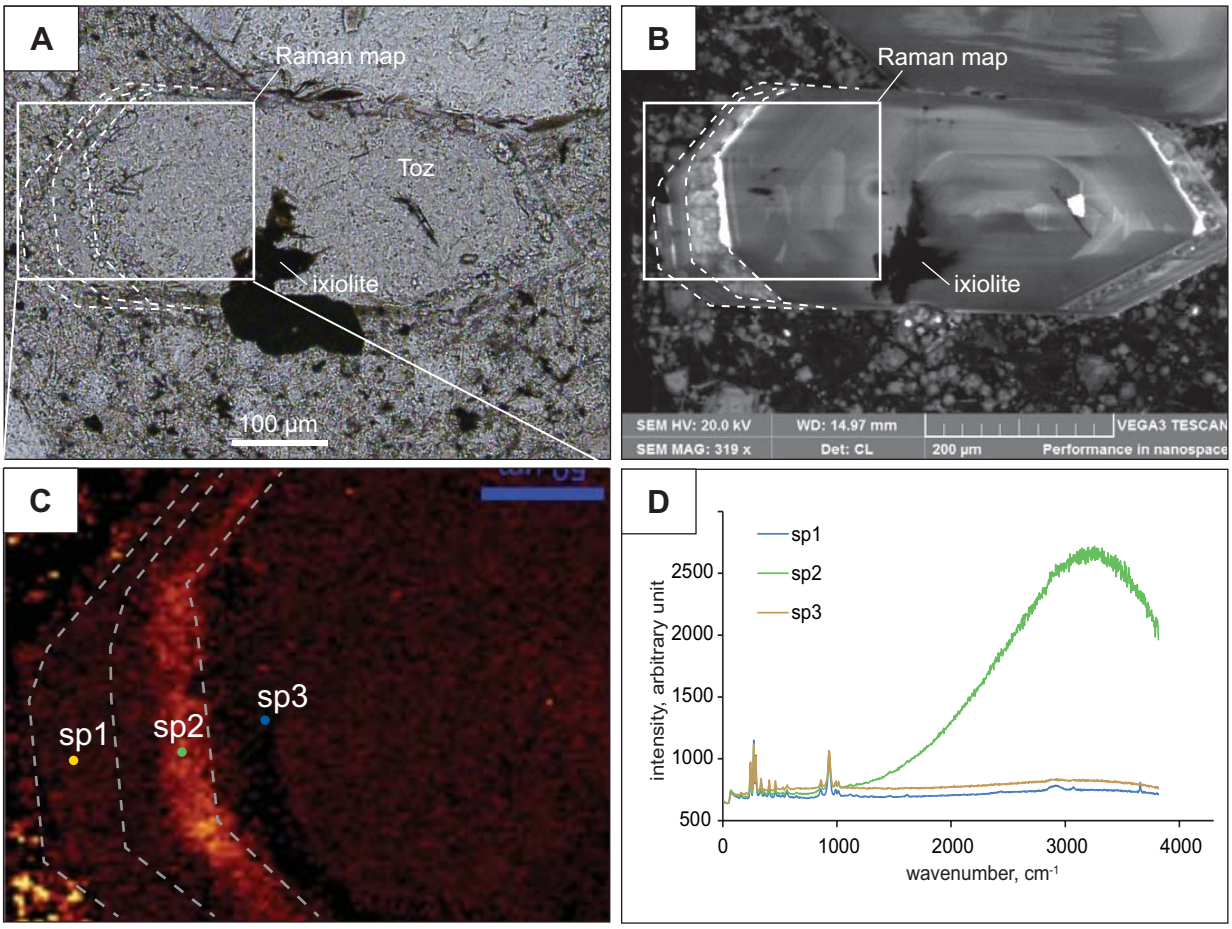
A
Raman map
Toz
ixiolite
100 μm
B
Raman map
ixiolite
SEM HV: 20.0 kV
WD: 14.97 mm
VEGA3 TESCAN
SEM MAG: 319 x
Det: CL
200 μm
Performance in nanospace
C
sp1
sp2
sp3
D
sp1
sp2
sp3
intensity, arbitrary unit
2500
2000
1500
1000
500
0
1000
2000
3000
4000
wavenumber, cm-1

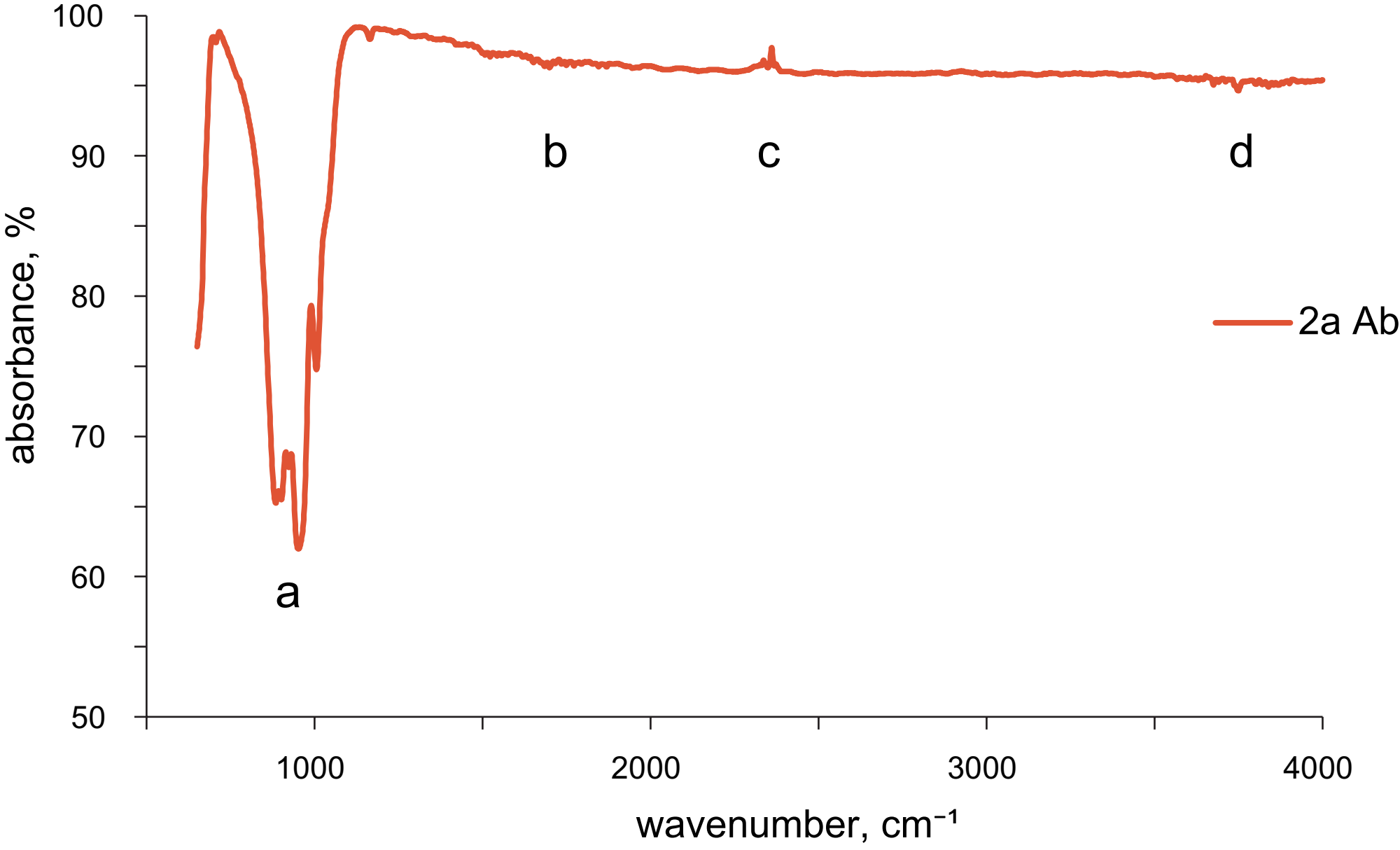
100
90
80
70
60
50
absorbance, %
a
b
c
d
2a Ab
1000
2000
3000
4000
wavenumber, cm⁻¹

Table 1 Luminescence emission centers in topaz and their peak assigments.

Peak Position (nm)	Peak Assignment	Reference	Method
393		this study	SEM-CL/Room Temp
480	OAl* point defect	Correcher et al. 2011	TL-CL/Room and Low Temp
410	$O^{-}(Al_2)$ centre in an irradiated sample	Da Silva et al (2005)	Optical absorption
455	Ti^{4+}	Gaft et al. 1998	LIPL/Room Temp
460	paramagnetic O^{-} hole centre in an irradiated sample	Krambrock et al. (2007)	EPR/Optical absorption
620	$O^{-}(Al_2)$ centre in irradiated sample	Da Silva et al. (2005)	Optical absorption
650 (700)	Fe-related hole centre	Correcher et. 2011	TL-CL/Room and Low Temp
684	Cr^{3+}	Gaft et al. 1998	LIPL/Room Temp
711	Cr^{3+}	Gaft et al. 1998	LIPL/Room Temp
734	Cr^{3+}	Gaft et al. 1998	LIPL/Room Temp

Table 2. EPMA of topaz phenocrysts (all elements as wt.%)

Analysis	AB1_01	AB1_02	AB1_03	AB1_04	AB1_05	AB1_06	AB1_07	AB1_08	AB1_14	AB1_15	AB1_16	AB1_17	AB1_18
F	21.01	21.1	21.04	21.04	21.32	21.26	21.35	21.55	21.4	21.38	21.33	21.2	21.02
Na2O	0.03	0.01	0.01	0.01	0.03	bdl	bdl	0.02	0.01	0.01	bdl	bdl	bdl
MgO	bdl	bdl	bdl	bdl	bdl	bdl	bdl	0.01	bdl	bdl	bdl	0.01	bdl
Al2O3	56.04	55.9	56.57	56.37	56.31	56.38	55.8	55.92	55.73	56.03	56.11	56.42	56.06
SiO2	32.36	32.62	31.89	31.63	31.7	31.18	31.07	31.21	31.64	31.92	31.92	31.98	31.22
K2O	0.02	0.01	0.01	0.01	bdl	0.01	bdl	bdl	bdl	bdl	bdl	bdl	0.01
CaO	bdl	bdl	0.01	0.01	bdl	bdl	0.01	bdl	0.01	bdl	0.01	0.01	0.01
Cl	bdl	bdl	bdl	0.01	bdl	bdl	bdl	0.01	bdl	0.01	bdl	0.01	bdl
SO3	0.01	0.03	0.02	0.02	0.01	0.01	0.02	bdl	0.03	0.01	0.01	0.01	bdl
P2O5	bdl	bdl	0.02	bdl	bdl	bdl	0.01	0.02	bdl	0.03	0.03	0.04	bdl
FeO	0.01	0.02	bdl	0.02	bdl	0.01	0	bdl	bdl	bdl	bdl	bdl	0.04
TiO2	bdl	0.06	0.01	0.01	0.01	bdl	0.03	bdl	bdl	bdl	bdl	bdl	bdl
O=F , Cl	8.85	8.88	8.86	8.86	8.98	8.95	8.99	9.08	9.01	9.01	8.98	8.93	8.85
Total	100.64	100.86	100.73	100.28	100.41	99.9	99.31	99.66	99.81	100.39	100.44	100.75	99.51
H2O*	-	-	-	-	-	0.1	0.69	0.34	0.19	-	-	-	0.49

*calculated by difference (100-tot)

bdl below detection limit

Table 2 (continued)

Analysis	AB1_21	AB1_22	AB1_23	AB1_24	AB1_31	AB1_32	AB1_36	AB1_37	AB1_38	AB1_42	AB1_43	AB1_44	AB1_45
F	21.22	21.4	21.15	21.32	20.99	21.39	20.71	21.96	22.01	21.33	21.36	21.43	21.76
Na2O	0.02	0.02	bdl	bdl	0.04	0.01	bdl	0.02	0.01	0.01	bdl	0.01	bdl
MgO	0.01	0.02	bdl	bdl	bdl	bdl	bdl	bdl	bdl	bdl	bdl	bdl	bdl
Al2O3	56.43	56.04	56.18	56.17	56.15	56.45	56.11	55.92	56.13	56.19	56.34	56.43	56.4
SiO2	31.23	31.4	31.08	30.89	31.15	31.55	31.13	31.02	31.38	31.12	30.94	31.35	30.97
K2O	0.01	0.01	bdl	0.02	0.02	bdl	bdl	0.02	0.01	0	bdl	bdl	bdl
CaO	bdl	bdl	bdl	bdl	bdl	bdl	bdl	bdl	0.02	0.01	bdl	bdl	bdl
Cl	bdl	bdl	bdl	bdl	0.01	bdl	0.01	bdl	0.01	bdl	bdl	0.01	bdl
SO3	bdl	bdl	0.02	bdl	0.04	bdl	0.01	bdl	bdl	0.02	0.01	bdl	bdl
P2O5	0.03	0.01	0.01	0.07	0.02	0.02	0	bdl	0.01	bdl	bdl	bdl	0.04
FeO	bdl	bdl	0.01	bdl	bdl	0.03	0.04	0.02	0.06	0.03	0.01	bdl	bdl
TiO2	bdl	0.03	bdl	0.03	0.01	bdl	0.05	bdl	bdl	bdl	0.04	0.02	bdl
O=F , Cl	8.93	9.01	8.91	8.98	8.84	9.01	8.72	9.25	9.27	8.98	9	9.03	9.16
Total	100.01	99.91	99.56	99.53	99.59	100.44	99.34	99.73	100.37	99.73	99.7	100.23	100.02
H2O*	-	0.09	0.44	0.47	0.41	-	0.66	0.27	-	0.27	0.3	-	-

Table 2 (continued)

Analysis	AB1_46	AB1_47	AB1_09	AB1_12	AB1_13	AB1_19	AB1_20	AB1_27	AB1_39	AB1_40	AB1_41	AB1_49	AB1_50
F	21.32	21.54	22.15	22.49	21.75	21.27	21.47	21.55	21.97	21.62	21.52	21.72	22.29
Na2O	0.02	0.02	bdl	0.01	0.01	0.02	0.02	0.03	0.02	0.01	bdl	0.02	bdl
MgO	bdl	bdl	0.01	bdl	bdl	0.01	bdl	bdl	bdl	bdl	bdl	0.02	bdl
Al2O3	56.01	56.47	56.12	56.16	55.97	56.12	55.91	55.6	56.37	56.6	56.62	56.24	56.25
SiO2	31.14	31.01	31.28	31.19	31.28	30.74	30.84	31.32	31.1	31.8	31.51	31.42	31.18
K2O	bdl	0.01	bdl	0.02	bdl	0.02	0.03	0.01	0.02	0.02	0.01	0.02	0.01
CaO	0.02	0.01	0.02	bdl	0.01	bdl	0.01	0.02	0.01	bdl	bdl	0.01	bdl
Cl	bdl	0.01	bdl	bdl	0.01	bdl	bdl	bdl	0.01	0.01	bdl	0.01	0.02
SO3	0.01	0.02	0.01	bdl	0.01	0.01	bdl	bdl	0.01	0.01	0.01	0.01	bdl
P2O5	0.03	bdl	0.02	0.01	0.05	0.04	0.01	0.06	0.01	bdl	bdl	0.06	0.07
FeO	bdl	0.03	0.05	0.03	0.02	0.04	bdl	0.05	bdl	0.12	0.06	0.01	0.05
TiO2	bdl	bdl	0.03	0.02	0.04	bdl	0.04	0.05	bdl	bdl	bdl	bdl	bdl
O=F , Cl	8.98	9.07	9.33	9.47	9.16	8.96	9.04	9.07	9.25	9.11	9.06	9.15	9.39
Total	99.56	100.05	100.35	100.45	99.99	99.3	99.29	99.6	100.27	101.07	100.67	100.39	100.48
H2O*	0.44	-	-	-	0.01	0.7	0.71	0.4	-	-	-	-	-

Table 3. LA-ICP-MS analyses of topaz phenocrysts

Analysis	-10 core	-11 core	-12 core	-13 core	-14 core	-15 core	-16 core	-17 core	-18 core	-2 core	-20 core	-21 core	-23 core	-24 core	-25 core	-26 core	-28 core	-29 core
Li (ppm)	2.46	10.29	10.27	9.49	3.13	2.93	14.76	57.60	23.16	4.71	34.48	98.39	3.50	3.99	3.55	3.85	2.93	3.28
Na	<144.63	<138.05	<129.01	89312.7	490.05	577.10	<251.45	<201.05	<153.87	471.57	<96.87	<128.71	<193.44	282.94	<134.97	<143.74	163.31	<80.58
Mg	<2.48	<3.78	<3.99	21111.7	148.88	110.58	47.58	8.74	12.48	<3.65	<2.60	<3.30	<2.58	<3.37	<2.64	<2.67	8.81	<2.56
Al*	296700	296700	296700	296700	296700	296700	296700	296700	296700	296700	296700	296700	296700	296700	296700	296700	296700	296700
Si	136341	136492	133221	408053	139617	138040	139611	128968	134748	123579	136273	138862	134097	131851	133010	135435	134215	138692
P	<64.17	<42.90	<59.06	<89.85	<67.43	<76.05	<107.99	111.80	135.74	100.03	105.82	120.72	190.15	124.32	<54.44	<67.99	110.13	136.24
K	<8.47	17.77	<11.14	7403.89	52.57	54.30	35.35	<15.89	<11.30	<16.34	<8.79	<9.64	13.25	9.71	<10.40	<9.36	15.50	<8.73
Ca	747.00	<497.70	<673.64	39520.7	<602.43	666.11	754.85	<613.05	716.97	<634.80	510.78	<361.00	<425.29	789.09	518.79	<492.23	<330.33	495.71
Ti	4.23	12.96	14.79	104.80	6.71	<5.41	37.02	52.94	28.65	13.70	36.07	55.00	10.29	10.02	12.05	8.02	8.81	9.07
Mn	<6.44	<3.95	<5.43	<10.50	6.44	<5.98	13.60	<8.12	<6.27	<8.20	4.56	9.94	<8.13	<5.28	<6.52	<6.84	<4.12	6.60
Fe	25.77	22.13	<28.33	208.16	<28.82	28.70	91.75	93.36	60.11	<34.73	54.89	87.17	38.39	31.35	<24.55	<27.81	40.71	22.62
Ni	<0.40	<0.47	<0.59	<0.62	<0.33	<0.38	<1.15	<0.79	<0.57	<0.82	<0.33	<0.58	<0.60	<0.41	<0.52	<0.42	<0.54	<0.44
Ga	4.13	5.92	6.17	12.20	4.18	4.47	14.35	16.51	11.96	5.67	19.60	25.09	6.45	7.26	6.55	5.09	5.53	5.78
Y	<0.01	0.03	<0.02	1.05	<0.02	<0.03	<0.03	<0.05	<0.03	<0.02	0.02	<0.03	<0.04	<0.02	<0.02	<0.01	<0.01	<0.04
Zr	<0.03	0.04	<0.07	87.26	0.45	0.42	<0.11	<0.09	0.11	<0.04	0.04	<0.08	<0.02	<0.02	<0.02	<0.03	<0.03	<0.02
Nb	0.16	0.89	2.51	0.66	0.08	0.12	2.96	8.31	3.69	0.31	0.89	2.38	1.07	0.74	0.33	0.13	2.75	0.97
Sn	<0.13	<0.15	<0.09	0.33	<0.14	0.07	<0.21	0.32	<0.09	<0.18	<0.10	0.10	0.47	0.17	<0.13	<0.14	0.41	0.16
La	0.02	0.04	0.06	1.43	<0.02	<0.01	0.34	0.28	0.13	<0.02	0.35	0.61	0.04	0.03	0.02	<0.01	0.04	0.02
Ce	0.08	0.19	0.25	2.28	0.03	0.08	1.46	1.49	0.64	0.04	1.27	2.65	0.25	0.20	0.09	0.04	0.19	0.12
Nd	<0.07	<0.08	<0.09	0.77	<0.09	<0.08	0.17	0.39	<0.08	<0.11	0.17	0.59	<0.16	<0.07	<0.07	<0.08	<0.05	<0.06
Sm	<0.08	<0.09	<0.10	<0.14	<0.11	<0.09	<0.14	<0.14	<0.09	<0.26	<0.07	<0.08	<0.08	<0.08	<0.08	<0.19	<0.06	<0.07
Gd	<0.08	<0.09	<0.10	<0.14	<0.10	<0.09	<0.14	<0.14	<0.09	<0.13	<0.08	4014.00	<0.08	<0.08	<0.08	<0.19	<0.06	<0.07
Tb	<0.01	<0.01	<0.01	<0.02	<0.01	0.02	<0.02	<0.02	<0.01	<0.01	<0.01	<0.01	<0.01	<0.01	<0.01	<0.01	<0.01	<0.01
Yb	<0.06	<0.07	<0.08	<0.11	<0.08	<0.07	<0.22	<0.11	<0.15	<0.09	<0.05	<0.06	<0.06	<0.06	<0.06	<0.07	<0.05	<0.05
Lu	<0.01	<0.01	<0.02	0.03	<0.01	<0.01	<0.02	<0.02	<0.01	<0.01	<0.01	<0.01	<0.02	<0.01	<0.01	<0.01	<0.01	<0.02
Ta	0.04	0.42	0.86	0.11	0.02	0.04	1.60	4.43	2.20	0.21	0.27	0.82	0.44	0.33	0.12	0.05	1.12	0.47
W	0.22	0.60	2.66	0.39	0.07	0.24	2.59	9.23	3.84	0.08	8.60	14.80	0.79	0.84	0.36	0.06	0.56	0.51
Pb	<0.16	0.25	<0.17	6.67	<0.21	0.16	<0.27	<0.28	<0.1	<0.31	<0.21	0.09	0.22	<0.12	<0.08	<0.13	0.33	<0.09
Th	0.05	0.04	<0.03	0.49	<0.03	<0.05	0.25	0.27	0.08	<0.03	0.13	0.19	0.06	0.05	0.03	<0.02	<0.01	0.09
U	<0.02	<0.02	<0.02	0.21	<0.02	<0.02	<0.03	<0.03	<0.02	<0.03	<0.03	<0.01	<0.01	0.03	<0.02	<0.02	0.02	0.02

* internal standard

Table 3. (continued)

Analysis	-3 core	-31 core	-32 core	-33 core	-34 core	-35 core	-37 core	-4 core	-5 core	-6 core	-7 core	-9 core	-1 rim	-22 rim	-27 rim	-36 rim	-8 rim
Li (ppm)	2.78	3.86	1.97	2.86	2.45	2.11	2.55	2.63	2.45	2.05	3.01	4.60	9.86	160.78	34.12	8.74	42.62
Na	401.53	404.69	386.07	<122.61	110.69	<130.55	<114.04	<206.06	<202.38	<85.77	<193.41	<139.76	<173.25	606.56	<197.70	286.00	<209.46
Mg	<3.43	48.33	66.93	<2.99	<2.59	<2.37	<3.26	<2.33	<2.66	<2.40	<2.83	<3.79	<5.59	81.47	<5.72	<2.78	<4.16
Al*	296700	296700	296700	296700	296700	296700	296700	296700	296700	296700	296700	296700	296700	296700	296700	296700	296700
Si	122591	133007	132518	132996	136521	140775	135172	138151	133766	135400	131700	140059	151590	187096	211165	131560	190396
P	103.12	<76.94	<60.29	78.92	<49.57	60.42	<64.90	197.26	143.50	133.41	135.33	86.64	<93.56	117.67	152.31	<48.48	<88.42
K	<11.34	<13.53	24.14	<9.34	<7.75	<8.57	<10.63	<10.71	<11.06	<10.43	<11.43	<11.46	<11.65	1163.64	75.84	<11.24	<16.68
Ca	<453.15	<438.17	500.31	462.21	647.24	550.54	534.91	<502.27	451.35	<466.33	518.35	565.76	<604.82	3665.54	<623.19	<437.08	<662.97
Ti	13.26	10.50	14.55	14.68	5.88	4.06	5.46	4.98	6.34	4.15	8.25	<4.77	21.44	34.49	13.90	18.52	18.66
Mn	<10.42	<8.71	<7.28	<5.78	<4.45	10.27	<4.51	<7.43	<8.17	<3.94	<7.36	<5.78	<7.58	68.56	<7.39	<6.56	<6.79
Fe	<28.77	<21.72	<22.18	<23.80	<18.49	<20.39	<17.39	<23.77	<26.26	<19.77	<23.34	33.15	57.21	587.62	40.23	27.30	49.73
Ni	<0.64	<0.65	<0.48	<0.53	<0.43	<0.38	<0.54	<0.67	<0.46	<0.52	<0.26	<0.45	<1.32	1.06	<0.68	<0.52	<0.86
Ga	5.60	5.27	4.68	5.52	4.34	4.81	4.96	4.90	4.94	5.11	6.58	4.78	6.49	13.33	8.24	7.78	8.11
Y	<0.01	0.06	<0.02	<0.04	<0.03	<0.01	<0.03	0.02	0.02	<0.02	<0.03	<0.02	<0.02	0.30	0.05	<0.05	0.10
Zr	<0.03	0.20	0.16	<0.02	<0.02	<0.02	<0.02	<0.02	<0.02	<0.02	<0.02	<0.03	<0.05	0.87	0.07	<0.03	0.32
Nb	0.24	0.22	2.14	2.83	0.38	0.13	0.78	0.13	0.09	0.08	0.06	0.16	0.69	11.74	2.02	7.12	1.12
Sn	0.09	0.07	0.07	<0.16	0.06	<0.04	<0.14	<0.11	<0.15	<0.09	<0.11	0.10	0.52	4.41	0.71	0.25	0.73
La	<0.01	0.07	<0.01	<0.01	<0.01	<0.01	<0.01	<0.01	<0.01	<0.01	<0.01	0.03	0.03	1.11	0.12	0.36	0.21
Ce	<0.01	0.21	0.06	<0.01	<0.01	<0.01	0.12	<0.01	<0.01	<0.01	0.03	0.13	0.15	4.37	0.48	1.71	1.01
Nd	<0.08	0.13	<0.07	<0.07	<0.06	<0.06	<0.07	<0.07	<0.14	<0.06	<0.14	<0.08	<0.13	1.09	0.11	0.26	0.35
Sm	<0.10	<0.09	<0.08	<0.08	<0.07	<0.07	<0.08	<0.08	<0.08	<0.08	<0.08	<0.10	<0.15	0.29	<0.25	<0.10	<0.13
Gd	<0.10	<0.09	<0.08	<0.08	<0.07	<0.07	<0.08	<0.08	<0.08	<0.08	<0.08	<0.10	<0.15	0.22	<0.12	<0.10	<0.13
Tb	<0.01	<0.01	<0.01	<0.01	<0.01	<0.01	<0.01	<0.01	<0.01	<0.01	<0.01	<0.01	<0.02	<0.01	0.02	<0.01	<0.01
Yb	<0.15	<0.07	<0.06	<0.06	<0.11	<0.05	<0.06	<0.06	<0.06	<0.06	<0.06	<0.07	<0.11	0.11	<0.09	<0.08	0.27
Lu	<0.01	<0.01	<0.01	<0.01	<0.01	<0.01	<0.01	<0.01	<0.01	<0.01	<0.013	<0.01	<0.02	<0.01	<0.01	<0.01	<0.01
Ta	0.20	0.08	1.42	1.25	0.18	0.06	0.26	0.12	0.03	0.03	0.01	0.05	0.47	5.49	0.95	3.06	0.49
W	0.14	0.29	0.06	0.21	0.05	0.05	0.23	0.05	0.05	0.05	0.48	0.41	0.34	10.89	1.70	3.36	5.13
Pb	<0.19	<0.16	<0.10	<0.14	<0.12	0.11	<0.11	0.23	0.12	<0.09	<0.13	<0.17	0.18	0.93	<0.19	<0.15	0.90
Th	<0.02	0.15	<0.04	<0.04	<0.01	<0.01	<0.02	<0.02	<0.02	<0.05	<0.02	0.07	0.16	2.23	0.17	0.38	2.38
U	<0.02	0.03	<0.02	<0.01	<0.01	<0.03	<0.01	<0.01	<0.01	<0.01	<0.01	<0.02	0.04	0.24	<0.06	<0.02	0.30